and length about 2–3 μm. Metal chelate precursors, $M(hfa)_2{\cdot}xH_2O$ (M = Pd, Ni, and Cu; hfa = hexafluoroacetylacetonate) were purchased from Aldrich Chemical Company and used as received. For palladium impregnation, 10 mg of MWCNTs were loaded in a 3.47 mL high pressure stainless reactor along with 10–50 mg of $Pd(hfa)_2{\cdot}xH_2O$. The first valve, V_1, was closed while valves V_2, V_3, and V_4 were opened and 3 atm of H_2 flowed through the reactor for 5 min to expel the air inside. Valves V_2, V_3, and V_4 were then closed, and V_1 was opened to purge the mixer with 80 atm of CO_2. V_1 was closed again after CO_2 purging. CO_2 and H_2 were mixed well by magnetic stirring. Valves V_1 and V_3 were opened, pumping CO_2 and H_2 mixture into the reactor, and then closed. After 30 min, the precursor was dissolved completely in CO_2, and a uniform solution was obtained. Then the reactor was heated gradually to 80–150 °C and the temperature was maintained for about 5 min. After that, the reactor was cooled to 35 °C, and vented slowly by opening V_4. CO_2 flow was used to flush the reactor twice to remove the possible unreacted species and by-products. The reactor was then opened, and the recovered powders were subjected to TEM and EDS analyses. The same procedure and conditions were also adopted for filling nickel and copper into MWCNTs, except that the reactor was heated to a higher temperature, i.e., 250 °C. High-resolution TEM analysis was carried out on a Jeol JEM 2010 microscope with a routine point-to-point resolution of 0.194 nm. The operating voltage on the microscope was 200 keV. All images were digitally recorded with a slow scan charge coupled device (CCD) camera (image size 1024 × 1024 pixels) and image processing was carried out using a Digital Micrograph (Gatan). EDS analysis was carried out on an Oxford ISIS system attached to the Jeol 2010 TEM.

Received: June 6, 2002
Final version: November 30, 2002

[1] P. M. Ajayan, *Chem. Rev.* **1999**, *99*, 1787.
[2] J. Hu, T. W. Odom, C. M. Lieber, *Acc. Chem. Res.* **1999**, *32*, 435.
[3] J. Liu, A. G. Rinzler, H. Dai, J. H. Hafner, R. K. Bradley, P. J. Boul, A. Lu, T. Liverson, K. Shelimov, C. B. Huffman, F. Rodriguez-Macias, Y.-S. Shon, T. R. Lee, D. T. Colbert, R. E. Smalley, *Science* **1998**, *280*, 1253.
[4] E. W. Wong, P. E. Sheehan, C. M. Lieber, *Science* **1997**, *277*, 1971.
[5] S. J. Tans, M. H. Devoret, H. Dai, A. Thess, R. E. Smalley, L. J. Geerligs, C. Dekker, *Nature* **1997**, *386*, 474.
[6] J. T. Hu, O. Y. Min, P. D. Yang, C. M. Lieber, *Nature* **1999**, *399*, 48.
[7] S. J. Tans, A. R. M. Verschueren, C. Dekker, *Nature* **1998**, *393*, 49.
[8] S. Saito, *Science* **1997**, *278*, 77.
[9] R. M. Baum, *Chem. Eng. News.* **1997**, *75*, 39.
[10] Z. L. Liu, X. H. Lin, J. Y. Lee, W. D. Zhang, M. Han, L. M. Gan, *Langmuir* **2002**, *18*, 4054.
[11] Y. Lin, A. M. Rao, B. Sadanadan, E. A. Kenik, Y. P. Sun, *J. Phys. Chem. B* **2002**, *106*, 1294.
[12] S. C. Tsang, Y. K. Chen, P. J. F. Harris, M. L. H. Green, *Nature* **1994**, *372*, 159.
[13] S. Banerjee, S. S. Wong, *Nano Lett.* **2002**, *2*, 195.
[14] J. M. Planeiz, N. Coustel, B. Coq, V. Brotons, P. S. Kumbhar, R. Dutartre, P. Geneste, P. Bernier, P. M. Ajayan, *J. Am. Chem. Soc.* **1994**, *116*, 7935.
[15] P. Calvert, *Nature* **1992**, *357*, 365.
[16] P. M. Ajayan, S. Iijima, *Nature* **1993**, *361*, 333.
[17] J. Li, M. Moskovits, T. L. Haslett, *Chem. Mater.* **1998**, *10*, 1963.
[18] L. M. Ang, T. S. A. Hor, G. Q. Xu, C. H. Tung, S. Zhao, J. L. S. Wang, *Chem. Mater.* **1999**, *11*, 2115.
[19] R. Yu, L. Chen, Q. Liu, J. Lin, K. L. Tan, S. C. Ng, H. S. O. Chan, G. Q. Xu, T. S. A. Hor, *Chem. Mater.* **1998**, *10*, 718.
[20] T. W. Ebbesen, H. Hiura, M. E. Bisher, M. M. J. Treacy, J. L. Shreeve-Keyer, R. C. Haushalter, *Adv. Mater.* **1996**, *8*, 155.
[21] B. K. Pradhan, T. Toba, T. Kyotani, A. Tomita, *Chem. Mater.* **1998**, *10*, 2510.
[22] T. Kyotani, L. Tsai, A. Tomita, *Chem. Commun.* **1997**, 701.
[23] G. Che, B. B. Lakshmi, C. R. Martin, E. R. Fisher, *Langmuir* **1999**, *15*, 750.
[24] V. Lordi, N. Yao, J. Wei, *Chem. Mater.* **2001**, *13*, 733.
[25] M. Freemantle, *Chem. Eng. News* **1996**, *74*, 62.
[26] J. Cook, J. Sloan, M. L. H. Green, *Chem. Ind.* **1996**, *16*, 600.
[27] T. W. Ebbesen, *Phys. Today* **1996**, *June*, 26.
[28] J. Kong, N. R. Franklin, C. W. Zhou, M. G. Chapline, S. Peng, K. J. Cho, H. J. Dai, *Science* **2000**, *287*, 622.
[29] J. Kong, M. G. Chapline, H. J. Dai, *Adv. Mater.* **2001**, *13*, 1384.
[30] R. Sen, A. Govindaraj, C. N. R. Rao, *Chem. Mater.* **1997**, *9*, 2078.
[31] C. Guerret-Piecourt, Y. Le Bouar, A. Loiseau, H. Pascard, *Nature* **1994**, *372*, 761.
[32] S. W. Liu, J. J. Zhu, Y. Mastai, I. Felner, A. Gedanken, *Chem. Mater.* **2000**, *12*, 2205.
[33] U. Ugarte, A. Chatelain, W. A. de Heer, *Science* **1996**, *274*, 1897.
[34] E. Dujardin, T. W. Ebbesen, H. Hiura, K. Tanigaki, *Science* **1994**, *265*, 1850.
[35] A. Chu, J. Cook, R. J. R. Heeson, J. L. Hutchison, M. L. H. Green, J. Sloan, *Chem. Mater.* **1996**, *8*, 2751.
[36] K. Matsui, B. K. Pradhan, T. Kyotani, A. Tomita, *J. Phys. Chem. B* **2001**, *105*, 5682.
[37] B. Lakshmi, E. R. Fisher, C. R. Martin, *Nature* **1998**, *393*, 346.
[38] W. K. Hsu, S. Trasobares, H. Terrones, M. Terrones, N. Grobert, Y. Q. Zhu, W. Z. Li, R. Escudero, J. P. Hare, H. W. Kroto, D. R. M. Walton, *Chem. Mater.* **1999**, *11*, 1747.
[39] A. Govindaraj, B. C. Satishkumar, M. Nath, C. N. R. Rao, *Chem. Mater.* **2000**, *12*, 202.
[40] J. A. Darr, M. Poliakoff, *Chem. Rev.* **1999**, *99*, 495.
[41] F. Cansell, B. Chevalier, A. Demourgues, J. Etourneau, C. Even, Y. Garrabos, V. Pessey, S. Petit, A. Tressaud, F. Weill, *J. Mater. Chem.* **1999**, *9*, 67.
[42] C. M. Wai, F. Hunt, N. Smart, Y. Lin, *US Patent 6 132 491*, **2000**.
[43] X. R. Ye, C. M. Wai, *J. Chem. Educ.* **2003**, in press.
[44] X. R. Ye, C. M. Wai, D. Zhang, Y. Kranov, D. McIlroy, Y. Lin, M. Engelhard, *Chem. Mater.* **2003**, *15*, 83.
[45] J. M. Blackburn, D. P. Long, A. Cabanas, J. J. Watkins, *Science* **2001**, *294*, 141.
[46] J. J. Watkins, J. M. Blackburn, T. J. McCarthy, *Chem. Mater.* **1999**, *11*, 213.
[47] J. J. Watkins, J. M. Blackburn, D. P. Long, J. L. Lazorcik, *WO Patent 2001032951*, **2001**.
[48] J. M. Blackburn, D. P. Long, J. J. Watkins, *Chem. Mater.* **2000**, *12*, 2625.
[49] D. P. Long, J. M. Blackburn, J. J. Watkins, *Adv. Mater.* **2000**, *12*, 913.
[50] N. E. Fernandes, S. M. Fisher, J. C. Poshusta, D. G. Vlachos, M. Tsapatsis, J. J. Watkins, *Chem. Mater.* **2001**, *13*, 2023.
[51] N. R. B. Coleman, M. A. Morris, T. R. Spalding, J. D. Holmes, *J. Am. Chem. Soc.* **2001**, *123*, 187.
[52] N. R. B. Coleman, N. O'Sullivan, K. M. Ryan, T. A. Crowley, M. A. Morris, T. R. Spalding, D. C. Steytler, J. D. Holmes, *J. Am. Chem. Soc.* **2001**, *123*, 7010.
[53] W. Z. Li, J. G. Wen, Y. Tu, Z. F. Ren, *Appl. Phys. A* **2001**, *73*, 259.

High-Energy Photonic Bandgap in Sb_2S_3 Inverse Opals by Sulfidation Processing**

By *Beatriz H. Juárez*, *Marta Ibisate*, *José M. Palacios*, and *Cefe López**

Self-assembly colloidal crystal methods[1–3] have lately attracted great attention since macroporous silica or polystyrene spheres templates were found to show advantageous optical properties for building three-dimensional (3D) photonic crystals.[4]

These systems present a periodic modulation of the dielectric constant that result in a strong enhancement of its diffractive properties and the appearance of stop bands for light propagation, called photonic bandgaps (PBG).[5,6] When such a stop band remains unchanged in energy irrespective the direction of light propagation, a full PBG is achieved. A full

[*] Dr. C. López, B. H. Juárez, M. Ibisate
Instituto de Ciencia de Materiales de Madrid (CSIC)
Cantoblanco, E-28049 Madrid (Spain)
and Unidad Asociada UPV-CSIC
Camino de Vera s/n, E-46022 Valencia (Spain)
E-mail: cefe@icmm.csic.es
Dr. J. M. Palacios
Instituto de Catálisis y Petroleoquímica (CSIC)
Cantoblanco, E-28049 Madrid (Spain)

[**] This work was partially financed by the Spanish CICyT project MAT2000-1670-C04 and the European Commission Project IST-1999-19009 PHOBOS. The authors thank Prof. F. Meseguer and Prof. J. Sánchez-Dehesa for support.

  0935-9648/03/0302-0319 $ 17.50+.50/0

ADVANCED MATERIALS

PBG is required for light waveguides with low-losses and thresholdless lasers. Photolithography,[7] holography,[8] nanorobotic manipulation,[9] and self-assembly[1] methods, comprise the chief options to manufacture photonic crystals.

One of the significant requirements to develop a full PBG is the existence of a high dielectric function contrast in the crystal. In this way, Sözüer and coworkers[10] proved the existence of a full PBG in face-center cubic (fcc) arrays of air spheres immersed in a high dielectric constant medium ($\varepsilon_m > 8.4$).[11] For this reason, 3D macroporous silica or polystyrene opals, are widely used as supports in order to fill the interconnected cavities with materials possessing a high dielectric function. Silica or polystyrene matrices can then be finally removed by means of chemical etching or thermal treatment. In this case, the remaining structures are known as inverse opals,[12–14] and consist of air spheres in a high dielectric constant medium showing the negative replica of the initial fcc lattice. Porous silica matrices have been successfully infiltrated by chemical bath deposition (CBD) and chemical vapor deposition (CVD) methods. It is well known that synthesis methods involving gas reactants lead to syntheses with better materials quality: silicon[15] and germanium[16] are two very good examples. Due to the limitation imposed by the required high dielectric constant, there are very few materials capable of showing a full PBG. In silicon and germanium inverse opals a full PBG is predicted in the near infrared (NIR) range of the spectrum.

However, the existence of a limited number of transparent materials in the visible light region possessing a high dielectric constant decreases the chance of finding materials exhibiting a full PBG in this spectral range. Sb_2S_3 fulfils the optical requirements to obtain a PBG in the visible or the NIR, depending on its amorphous or crystalline nature.[17] The electronic gap of Sb_2S_3 lies around 2.2 eV (564 nm) for amorphous and 1.78 eV (697 nm) for crystalline Sb_2S_3 thin films.[18] The maximum values of the dielectric function are 10.9 and 14.4 for the amorphous and crystalline forms respectively.[17] Therefore, Sb_2S_3 inverse opals with a full PBG are a very important target in photonic crystal research.

For the synthesis of these structures, a modified chemical bath deposition (CBD) method has been employed showing promising results.[19] Although the quality of the material obtained by the wet method is very good, the control on the degree of infiltration and the uniformity of the composite can only be improved by substituting as many liquid phase precursors as possible for similar ones entering the reaction in gas phase. Here, we report on a two-reaction procedure in which a gas phase is the trigger of the reaction to grow crystalline Sb_2S_3 in opals. This newly developed method includes the hydrolysis and condensation of an antimony alkoxide precursor within the opal matrix, sulfidation of the hydrolyzed product (antimony oxide, Sb_2O_3), and finally chemical etching for silica removal. This method yields inverted samples of remarkable quality with greatly improved optical properties. The wet impregnation of a pure liquid precursor benefits the complete opal infiltration (because of its liquid nature) and produces the maximum amount of solid oxide after the hydrolysis reaction (because of not being dissolved). During the second reaction, the gas phase assures a better diffusion of the reactant for the chemical conversion.

We present the reflectance response of crystalline Sb_2S_3 inverse opals synthesized by using this method showing a broad and flat peak centered at ca. 760 nm, with an 85 % reflectivity that can be assigned to the full PBG. The full width at half maximum of this peak when recorded from the (111) direction is 100 nm, which corresponds to 14 % width-to-center ratio.

The sulfidation of the hydrolyzed precursor was performed in an upflow fixed-bed quart reactor at atmospheric pressure and 300 °C.

Thermodynamic data allows us to predict that the sulfidation of Sb_2O_3 at the operating conditions used is highly favored ($\Delta G^\circ_{573} = -31$ Kcal mol^{-1}) through an exothermic reaction ($\Delta H^\circ_{573} = -32$ Kcal mol^{-1}). Silica, however, cannot be affected by this sulfidation process. A variation of the operating conditions (temperature, flow rate of H_2S as a reactant, etc.) allows different rates of sulfide growth, leading to the formation of both amorphous and well-crystallized Sb_2S_3.

Incidentally, the spherical morphology of the beads and mechanical and sulfidation properties of Sb_2O_3 silica composites make them potentially suitable for the development of sorbents of H_2S.[20,21]

The synthesis of crystalline Sb_2S_3 inverse opals involves several steps. In the first stage, it is necessary to obtain a Sb_2O_3 silica composite for further sulfidation. Porous silica was impregnated with liquid antimony triethoxide, $Sb(OEt)_3$, under vacuum conditions. This opal was then exposed to a moist atmosphere at room temperature, promoting the hydrolysis of antimony triethoxide to antimony oxide Sb_2O_3 through the reaction:

$$2\,Sb(OEt)_3 + 3\,H_2O \rightarrow Sb_2O_3 + 6\,EtOH \quad (1)$$

Ethanol, as a hydrolysis product, was removed by vaporization by heating up the samples to 100 °C. Three successive impregnations of $Sb(OEt)_3$, followed by further hydrolysis, provided an infilling degree of nearly 90 % of Sb_2O_3. Due to the different molar volume of Sb_2O_3 and Sb_2S_3, an expansion is expected after the conversion. The Sb_2O_3 silica composites were subsequently sulfidated in a fixed-bed reactor at atmospheric pressure and 300 °C. The involved chemical reaction is:

$$Sb_2O_3 + 3\,H_2S_{(g)} \rightarrow Sb_2O_3 + 3\,H_2O \quad (2)$$

Scanning electron microscopy (SEM) images of the prepared Sb_2O_3–silica and Sb_2S_3–silica composites are shown in Figures 1a and 1b, respectively. During impregnation, the liquid alkoxide filled the interstitial cavities among silica spheres. After hydrolysis and condensation, the deposited solid Sb_2O_3 fills these cavities, as can be seen in Figure 1a. The presence of holes is due to the applied cleavage for sample

  0935-9648/03/0302-0320 $ 17.50+.50/0

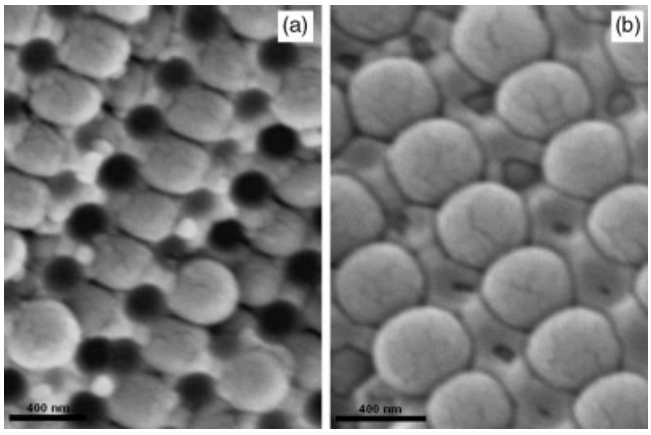

Fig. 1. SEM images of a) Sb_2O_3–silica and b) Sb_2S_3–silica composites.

preparation, but it is worth mentioning that the interstitial filling is shown to be complete and homogenous. Figure 1b shows the appearance of a sulfide–silica composite after sulfidation of the oxide.

To obtain a full PBG photonic material, opal inversion is subsequently required. This new structure is just the negative replica of the original opal, as silica spheres are removed by chemical etching. In this inverted opal, interconnected air spheres embedded in a Sb_2S_3 matrix provide enough contrast in the dielectric function to open a full PBG. The method used for silica removal is chemical treatment with a hydrofluoric solution (1 wt.-% in concentration) for seven hours. Figure 2 shows the appearance of the inverted opal after chemical

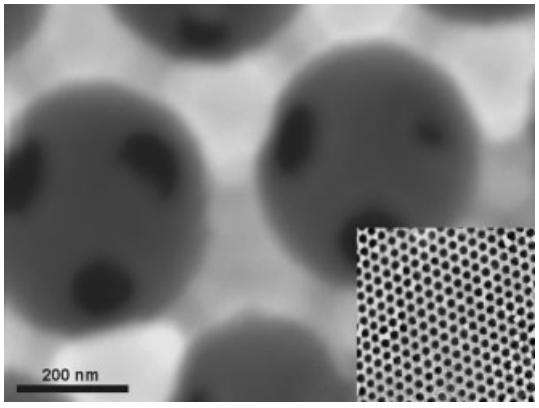

Fig. 2. SEM image of a (111) facet of a Sb_2S_3 inverted sample. The inset shows a lower magnification image.

etching. A high degree of connectivity between voids and high fidelity to the original opal is evidenced in large areas of the sample. It is worth mentioning the remarkable quality of both composites and inverted samples, as can be appreciated from the SEM images.

The composition of the inverted opals was determined in an SEM coupled to an energy dispersive X-ray (EDX) spectrometer. The respective Sb and S concentrations were found using a commercial Sb_2S_3 99.999 % purity as standard. The obtained composition of the inverted opal was very close to that expected for the stoichiometric antimony sulfide Sb_2S_3.

Further assessment of the chemical nature and structure of the compounds formed at the different stages of preparation has been achieved by powder X-ray diffraction (XRD). To minimize the detrimental effect derived from the presence of amorphous silica in oxide–silica composites, bulk hydrolyzed alkoxide was obtained by using identical operating conditions to those used in the preparation of hydrolyzed opals. To study the structural changes involved in the sulfidation of Sb_2O_3, bulk hydrolyzed precursor was sulfidated in the reactor together with Sb_2O_3–silica composite. Two different runs were performed using reaction times of six and ten hours. Operating temperature, gas flow rate, and pressure were kept constant for both experiments. The respective XRD patterns were processed using Rietveld methods, allowing the refinement of different structural parameters from the starting structure, including lattice and peak shape parameters. In addition, this method allows quantitative analysis of the crystalline chemical species found. The application of this method also reveals that the material lattice parameters underwent relevant changes (not shown). The conversion of oxidic into sulfided phase implies an increase in the molar volume that can account for crack development if a complete filling of voids in the preceding stage of preparation is achieved and depending on the operating conditions used during the sulfidation procedure. For this reason, incomplete infilling was used in the preceding stage of preparation.

In the ten-hour sulfidation test, the XRD pattern reveals that a 4 wt.-% of the oxide was present. However, the final inverted opal does not contain any traces of oxide, since Sb_2O_3 remnants are removed together with silica during chemical etching with HF. Experiments to remove silica spheres in Sb_2O_3–silica composites before sulfidation processing failed. The 1 wt.-% HF solution dissolved not only the silica, but also the Sb_2O_3 in the voids.

Figure 3a shows XRD pattern with well-defined reflections assigned to cubic Sb_2O_3 senarmonite. The presence of a broad peak centered at $2\theta = 28°$ suggests the partial presence of amorphous Sb_2O_3. The powder XRD pattern for the sulfi-

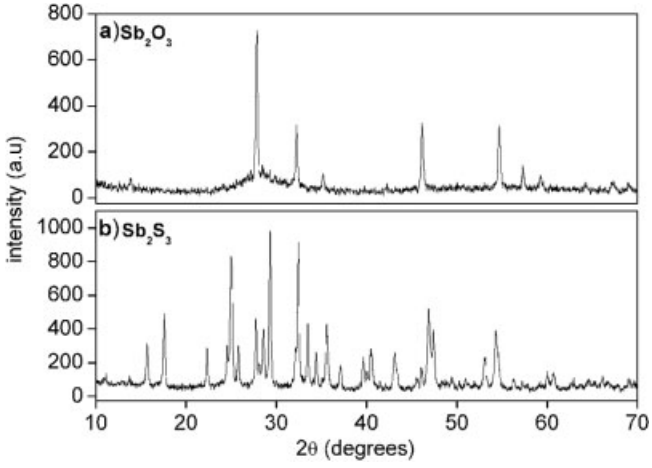

Fig. 3. XRD diffractograms from hydrolyzed $Sb(OEt)_3$: cubic senarmonite Sb_2O_3 (a), and from the latter after sulfidation: Sb_2S_3 (b).

  0935-9648/03/0302-0321 $ 17.50+.50/0

ADVANCED MATERIALS

dated compound is shown in Figure 3b. Narrow reflections show the crystalline nature of this sample comprised 96 wt.-% Sb_2S_3 and 4 wt.-% Sb_2O_3.

Optical reflectance spectra were obtained in several stages of sample preparation to track the filling degree of voids in bare opal. Since the position of the Bragg peak is a function of the dielectric constants of both the silica and the medium occupying the voids, material infiltration entails a shift of the diffraction peak.[22]

Plots in Figure 4 show the reflectance spectra for a bare opal before and after the first precursor condensation. Using a dielectric constant of 4.4 for the oxide, an estimate of the degree of infilling can be made. In this case, after the first condensation cycle, 65 % of the pore volume was filled with Sb_2O_3.

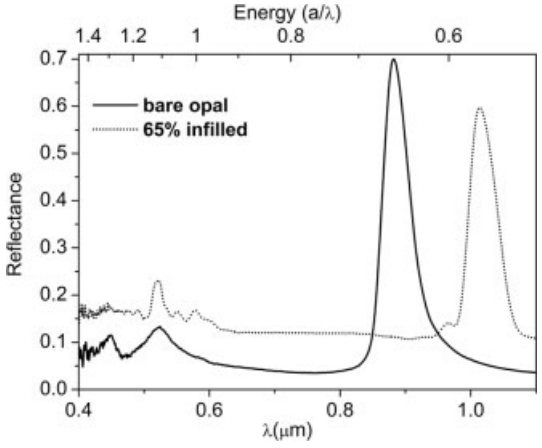

Fig. 4. Reflectance spectrum from a Sb_2O_3–silica composite. The shift in the first stop band is used to assess the degree of infiltration.

Optical properties for sulfide composite and inverted opal were also monitored with the support of band structure calculations.[23] Figure 5 shows theoretical calculations and experimental reflectance spectrum for a 100 % Sb_2S_3 infilled opal. Sb_2S_3 silica composite shows a broad and well-defined peak at low energy corresponding to the first stop band opened around the L point of the reciprocal lattice, the Bragg reflection peak. Again, from the position of this peak it is possible to assess the degree of infilling, because this peak shifts to higher wavelengths and broadens as the Sb_2O_3 becomes sulfidated. This fact is a consequence of the increase in the dielectric constants ratio as the oxide is replaced by sulfide as sulfidation proceeds.

Two extra peaks appear at higher energies that are in good agreement with theoretical calculations.

Figure 6 shows the band structure and the reflectance spectrum for the inverse structure made of crystalline Sb_2S_3. Clear correspondence can be established between the experimental peaks and gaps in the calculated bands. The marked region corresponds to the predicted full PBG in the inverted opal. This broad and well-defined peak is centered at 760 nm. The shape and high absolute reflectivity (85 %) of this peak confirms the quality of the sample. To assure the existence of the full PBG, a detailed study in other crystallographic directions is required, which will be the subject of future work.

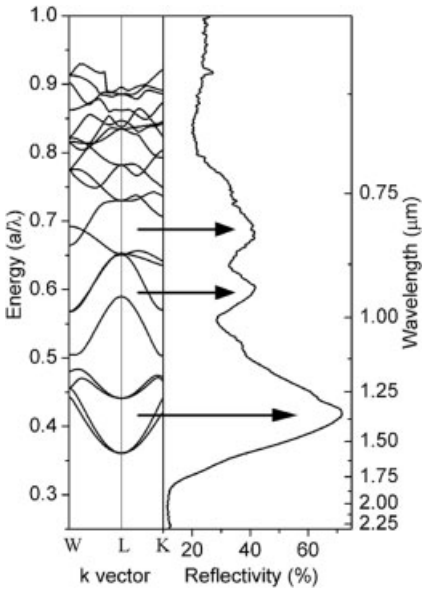

Fig. 5. Reflectance spectrum form a 410 nm diameter sphere loaded to a 100 % of the pore volume with Sb_2S_3 and band structure calculations for a 100 % infilled opal.

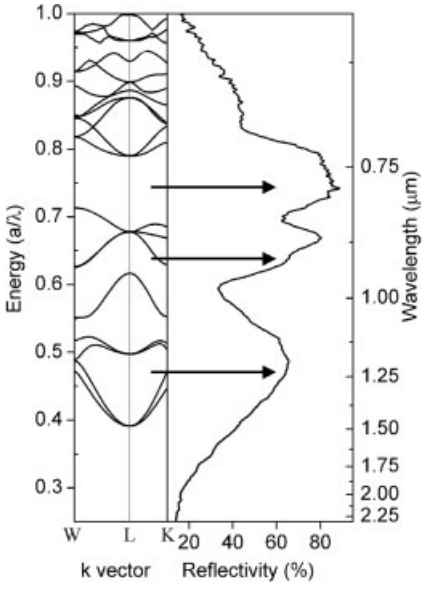

Fig. 6. Reflectance spectra from crystalline Sb_2S_3 inverse opal made of 410 nm sphere diameter and the band structure for a crystalline Sb_2S_3 inverted opal.

In summary, large Sb_2S_3 inverse opals have been prepared by hydrolysis of an ethoxy precursor and sulfidation followed by chemical etching. The optical characterization confirms the extraordinary photonic behavior of this material. A wide and well-defined peak in the reflectance spectrum in the range 700–800 nm defines the existence of the most energetic full PBG described in the literature. The homogeneity and degree of infiltration of the samples improve on the antimony trisulfide inverse opals prepared by CBD methods.

  0935-9648/03/0302-0322 $ 17.50+.50/0

Experimental

Opals shown in this work have been prepared following a method described previously [1,24]. This sol–gel method provides size-controlled spheres for further sedimentation by gravity. The sediments are sintered (thermal annealing at 950 °C for 3 h) to control the lattice parameter (*a*), and to strengthen the structures for consequent infillings. The usual size of the opal bits used for infiltration is 5–9 mm^2 in surface area by 0.5 mm thickness. The sphere diameter is 410 nm and, accordingly, the lattice parameter $a = 580$ nm.

Fixed-Flow Reactor: Sb_2O_3-silica composites were placed in the bottom bed of an upflow fixed-bed quartz reactor at atmospheric pressure. The gas flow rate was kept constant at 34 mL min^{-1}. The composition of the reactant gas from cylinders controlled by mass flow controllers was 20 vol.-% H_2S in N_2.

Operating temperature and reaction time were the variables affecting the sulfide growth. Temperatures around 280–300 °C are considered optimal for the sulfidation. Samples cracks are apparent as the operating temperature rises up to 550 °C (melting point of Sb_2S_3). Sulfidation times of 10 h resulted in almost complete oxide conversion (96 %).

Band structure calculations were carried out by using the MIT package software. In this program, the fully vectorial Maxwell equations are solved for plane-wave propagation in a periodic dielectric medium. The system is characterized by the dielectric functions of the voids and backbone, the crystalline structure, and the value of the lattice parameter.

Optical Characterization: The measurements were performed with a Fourier transform infrared spectrometer (FTIR), IFS 66S from Bruker with a IRScope II microscope attached. A 36 X Cassegrain objective was used to focus and collect the light. The incident and collected light cover external angles from 15° to 30° from normal incidence with respect to (111) family of planes.

The X-ray powder diffraction (XRD) study was carried out in a Siemens 5000 diffractometer using Cu Kα radiation.

The reference sample is the commercial product from Aldrich, Antimony trisulfide 99 %+.

Received: October 15, 2002
Final version: November 28, 2002

[1] R. Mayoral, J. Requena, J. S. Moya, C. López, A. Cintas, H. Miquez, F. Meseguer, L. Vázquez, M. Holgado, A. Blanco, *Adv. Mater.* **1997**, *9*, 257.
[2] M. Holgado, F. García-Santamaría, A. Blanco, M. Ibisate, A. Cintas, H. Míguez, A. J. Serna, C. Molpeceres, J. Requena, A. Mifsud, F. Meseguer, C. López, *Langmuir* **1999**, *15*, 4701.
[3] P. Jiang, J. F. Bertone, K. S. Hwang, V. L. Colvin, *Chem. Mater.* **1999**, *11*, 2132.
[4] J. D. Joannopoulos, P. R. Villeneuve, S. Fan, *Nature* **1997**, *386*, 143.
[5] E. Yablonovitch, *Phys. Rev. Lett.* **1987**, *58*, 2059.
[6] S. John, *Phys. Rev. Lett.* **1987**, *58*, 2486.
[7] N. Yamamoto, S. Noda, A. Chutinan, *Jpn. J. Appl. Phys.* **1998**, *37*, L1502.
[8] M. Campbell, D. N. Sharp, M. T. Harrison, R. G. Denning, A. J. Tuberfield, *Nature* **2000**, *53*, 404.
[9] F. García-Santamaría, H. T. Miyazaki, A. Urquía, M. Ibisate, M. Belmonte, N. Shinya, F. Meseguer, C. López, *Adv. Mater.* **2002**, *16*, 1144.
[10] H. S. Sözüer, J. W. Haus, R. Inguva, *Phys. Rev B.* **1992**, *45*, 13 962.
[11] K. Busch, S. John, *Phys. Rev. E* **1998**, *58*, 3896.
[12] O. D. Velev, T. A. Jede, R. F. Lobo, A. M. Lenhoff, *Nature* **1997**, *389*, 448.
[13] J. Wijnhoven, W. L. Vos, *Science* **1998**, *281*, 802.
[14] A. A. Zakhidov, R. H. Baughman, Z. Iqbal, C. Cui, I. Khairulin, S. O. Dantas, J. Marti, V. G. Ralchenko, *Science* **1998**, *282*, 897.
[15] A. Blanco, E. Chomski, S. Grabtchak, M. Ibisate, S. John, S. W. Leonard, C. López, F. Meseguer, H. Míguez, J. P. Mondia, G. A. Ozin, O. Toader, H. M. van Driel, *Nature* **2000**, *405*, 437.
[16] H. Míguez, E. Chomski, F. García-Santamaría, M. Ibisate, S. John, C. López, F. Meseguer, J. P. Mondia, G. A. Ozin, O. Toader, H. M. van Driel, *Adv. Mater.* **2001**, *13*, 1634.
[17] G. Ghosh, B. P. Varma, *Thin Solid Films* **1979**, *60*, 61.
[18] M. T. S. Nair, Y. Peña, J. Campos, V. M. García, P. K. Nair, *J. Electrochem. Soc.* **1998**, *145*, 2113.
[19] B. H. Juárez, S. Rubio, J. Sánchez-Dehesa, C. López, *Adv. Mater.* **2002**, *14*, 1486.
[20] R. B. Slimane, J. Abbasian, *Fuel Process. Technol.* **2001**, *70*, 97.
[21] Z.-M. Wang, Y. S. Lin, *J. Catal.* **1998**, *174*, 43.
[22] H. Míguez, A. Blanco, F. Meseguer, C. López, H. M. Yates, M. E. Pemble, V. Fornés, A. Mifsud, *Phys. Rev. B* **1999**, *59*, 4563.
[23] S. G. Johnson, J. D. Joannopoulos, *Opt. Express* **2001**, *8*, 173
[24] W. Stöber, A. Fink, E. Bohn, *J. Colloid Interface Sci.* **1968**, *26*, 62.

Hydrogen-Assisted Thermal Evaporation Synthesis of ZnS Nanoribbons on a Large Scale**

By *Yang Jiang*, *Xiang-Min Meng*, *Ji Liu*, *Zhi-Yuan Xie*, *Chun-Sing Lee*, and *Shuit-Tong Lee**

Zinc sulfide, an important semiconductor compound of the IIB–VI groups, has a wide bandgap energy of 3.7 eV at 300 K. It has been used as base material for cathode-ray tube luminescent materials,[1] as efficient phosphors in flat-panel displays, in thin-film electroluminescent devices, and infrared (IR) windows.[2] Besides these applications there also have been some interests in the new mechano-optic applications, because ZnS doped with some metal cations is a promising material to emit intense light upon stress, a phenomenon known as triboluminescence.[3] In recent years, nanocrystalline ZnS has been reported to have some characteristics different from the bulk crystal,[4] which may extend its application range. Therefore, much attention has been focused on the synthesis of ZnS nanoparticles and films, and the exploration of their novel properties.[5–10] By comparison, one-dimensional ZnS nanomaterials, such as nanowires, nanorods, and whiskers, can be expected to exhibit special optical and electrical properties. Several approaches, e.g., liquid-crystal template,[11] irradiation,[12] and solvothermal[13] are available to obtain one-dimensional nanocrystalline ZnS.

More recently, a new distinct one-dimensional nanostructure with a rectangular cross section, called a nanoribbon[14] or nanobelt,[15] has been synthesized in semiconductor silicon[14] and oxides[15] directly by thermal evaporation at high temperature. Other efforts have been carried out to synthesize these ribbon-like nanostructures. Semiconducting SnO_2 nanoribbons have been obtained by oxidizing elemental Sn.[16] A quasi one-dimensional metal Zn nanostructure was obtained by thermal decomposition and deposition.[17] The synthesis of nanoribbons or nanobelts, particularly of the free-standing silicon nanoribbons, is intriguing, but appears to follow the oxide-assisted growth.[14] The ribbon-like nanostructures have been expected to represent important building blocks for nanodevices and offer exciting opportunities for both fundamental research and technological applications.

In this communication, we introduce a convenient hydrogen-assisted thermal evaporation method to synthesize nanoribbons of the semiconductor ZnS. The synthetic reaction was carried out in a quartz tube furnace using high-purity Ar pre-

[*] Prof. S.-T. Lee, Dr. Y. Jiang, Dr. X.-M. Meng, J. Liu, Dr. Z.-Y. Xie, Dr. C.-S. Lee
Center of Super-Diamond and Advanced Films (COSDAF) and Department of Physics and Materials Science
City University of Hong Kong
Tat Chee Avenue, Kowloon
Hong Kong, SAR (China)
E-mail: apannale@cityu.edu.hk

[**] The work was supported by a grant from the Research Grants Council of the Hong Kong SAR, China (Project No. CityU 3/01C (8730016)) and a Strategic Research Grant of the City University of Hong Kong (Project No. 7001175).

  0935-9648/03/0302-0323 $ 17.50+.50/0